Changes in Neovascular Lesion Hyperreflectivity After Anti-VEGF Treatment in Age-Related Macular Degeneration: An Integrated Multimodal Imaging Analysis

Giuseppe Casalino,[1,2] Francesco Bandello,[2] and Usha Chakravarthy[1]

[1]Ophthalmology Macular Service, Belfast Health and Social Care Trust and Centre for Experimental Medicine, Queen's University Belfast, Belfast, United Kingdom
[2]Department of Ophthalmology, Scientific Institute San Raffaele, Vita-Salute University, Milan, Italy

PURPOSE. To correlate presence of hyperreflective material (HRM) on spectral-domain optical coherence tomography (SD-OCT) with color fundus photography (CFP) in patients with different subtypes of neovascular age-related macular degeneration (n-AMD).

METHODS. Retrospective assessments were made at baseline and months 1, 3, and 12 after initiation of treatment. At baseline, CFP images were graded for the presence of blood, fibrin and lipid exudates, and retinal angiograms for n-AMD subtype. At the four selected visits, SD-OCT scans were graded for HRM type (well-defined or undefined) and location (subretinal, intraretinal, and subretinal pigment epithelium [RPE]), integrity of RPE, ellipsoid zone, and external limiting membrane (ELM).

RESULTS. A total of 121 eyes with active n-AMD from 117 patients were included. At baseline, undefined HRM was strongly associated with fibrin on CFP ($\chi^2 = 39.87$; $P < 0.001$). The overall prevalence of HRM decreased from 85.9% at baseline to 52.9% by month 12. From baseline to month 12, undefined HRM decreased (53.7% vs. 7.4%, respectively) and well-defined HRM increased (32.2% vs. 45.5%, respectively). Sub-RPE HRM, which was infrequent at baseline, increased up to 30.6% by month 12. At month 12, eyes with no HRM had the best mean final best-corrected visual acuity (BCVA), and those with undefined HRM the worst. Multivariate regression analysis showed that ELM disruption at both baseline and month 12 was a negative predictive factor for final BCVA ($P = 0.001$ and $P < 0.001$, respectively), whereas presence of subretinal fluid at month 12 and number of treatments were positive predictors for final BCVA ($P = 0.007$ and $P = 0.041$, respectively), but the covariates describing HRM did not reach statistical significance in these models.

CONCLUSIONS. In eyes with n-AMD, location and morphology of HRM changed after anti-VEGF treatment, and differences were observed in the various choroidal neovascularization (CNV) subtypes. After anti-VEGF treatment, it was well-defined HRM in the sub-RPE space that was observed mostly.

Keywords: color fundus photography, hyperreflective material, multimodal imaging, neovascular age-related macular degeneration, retinal angiography, spectral-domain optical coherence tomography

Age-related macular degeneration (AMD) is the leading cause of irreversible visual loss in people over 50 years of age in the developed world.[1] In the advanced stages of this disease, neovascularization of the macular tissues can lead to severe vision loss in more than 40% of patients by 3 years if left untreated.[2] Over the last decade, the advent of antivascular endothelial growth factor (anti-VEGF) treatment has dramatically changed the prognosis of neovascular AMD (n-AMD),[3] and the prevalence of blindness due to AMD has decreased.[4] However, the anatomical response to anti-VEGF treatment and the functional outcomes can vary markedly among patients with n-AMD. Many studies have revealed that the composition of the choroidal neovascularization (CNV) lesion influences the natural history as well as treatment-related functional and anatomical outcomes in eyes with AMD.[5]

Since the introduction of spectral-domain optical coherence tomography (SD-OCT), an improved differentiation of neovascular lesion components with more accurate visualization of the retinal layers, particularly at the level of photoreceptors and retinal pigment epithelium (RPE), has become possible.[6] The enhancement in OCT image resolution has helped to identify anatomical biomarkers to monitor and predict response to treatment.[7] Notably, the status of the ellipsoid zone (EZ) and the external limiting membrane (ELM) has been shown to correlate with functional outcomes following anti-VEGF treatment.[8,9] One recently identified OCT feature in n-AMD is areas of altered reflectivity (low and high) that obscure normal retinal anatomical features, and these changes were first attributed to neovascular components by Liakopoulos et al.[10] and Giani

TABLE 1. Initial and Final BCVA, Number of Treatments, Baseline, and Month-12 Frequency of Fibrin, Blood, and Lipid on Color Photography by Angiographic Subtype of Neovascular AMD

CNV	Age	Initial BCVA	Final BCVA	Number of Injections	Bsl Fibrin	Bsl Blood	Lipid Bsl	Fibrin at M-12	Blood at M-12	Lipid at M-12
Type 1	76.4 ± 7.4	66.5 ± 8.5	67.6 ± 11.6	7.8 ± 1.7	30.0%, 12/40	20.0%, 8/40	20.0%, 8/40	2.5%, 1/40	5.0%, 2/40	2.5%, 1/40
Type 2	77.2 ± 7.1	57.4 ± 14.1	64.8 ± 16.8	7.1 ± 1.9	70.8%, 17/24	58.3%, 14/24	4.2%, 1/24	0.0%, 0/24	4.2%, 1/24	4.2%, 1/24
Type 3	79.4 ± 6.5	54.8 ± 13	56.7 ± 16.9	6.7 ± 1.8	53.3%, 16/30	76.7%, 23/30	33.3%, 10/30	3.4%, 1/29	20.7%, 6/29	10.3%, 3/29
Mixed	80.5 ± 8.2	55.1 ± 15	63.9 ± 13.6	7.9 ± 1.3	73.3%, 11/15	46.7%, 7/15	20.0%, 3/15	6.7%, 1/15	6.7%, 1/15	13.3%, 2/15
PCV	73.2 ± 12.7	62.4 ± 15	71.7 ± 10.8	7.5 ± 2.7	41.7%, 5/12	91.7%, 11/12	41.7%, 5/12	0.0%, 0/12	8.3%, 1/12	16.7%, 2/12
Total	77.5 ± 8	59.9 ± 13.2	64.3 ± 14.9	7.4 ± 1.9	50.4%, 61/121	52.1%, 63/121	22.3%, 27/121	2.5%, 3/120	9.2%, 11/120	7.5%, 9/120

BCVA, best-corrected visual acuity; Bsl, baseline; M-12, month 12; CNV, choroidal neovascularization; PCV, polypoidal choroidal vasculopathy. At month 12, color photography was available for 120 eyes. Mean ± SD values are shown for the continuous variables of age, BCVA, and number of injections. The fractionated values refer to the relative frequency of the color photography findings in the different neovascular subtypes.

et al.[11] and were referred to as subretinal hyperreflective material (SHRM).[12] Although its exact composition is unclear, SHRM was reported to influence scar development and sustained loss of visual acuity in the Comparison of Age-related macular degeneration Treatments Trials (CATT) study.[13,14]

Anti-VEGF therapies result in marked morphologic improvements that can occur rapidly, but there is little information on the composition of SHRM and its evolution and rate of disappearance.

To better understand the relationships between the OCT characteristic of HRM and lesion composition, we undertook systematic multimodal grading of an image dataset before commencement of anti-VEGF therapy and after treatment and report the findings.

MATERIALS AND METHODS

Study Design

This was a retrospective analysis of clinical data acquired from patients with n-AMD at a single tertiary referral center in Belfast, Northern Ireland, UK. This study was performed in accordance with the tenets of the Declaration of Helsinki after approval by the institutional ethics committee.

Population and Study Protocol

We identified 1087 new patients in the electronic medical care records, who had attended the clinic between May 2012 and January 2014. In our clinic, all patients undergo comprehensive ocular examination, including best-corrected visual acuity (BCVA), evaluated using the Early Treatment Diabetic Retinopathy Study (ETDRS) chart; multimodal imaging, including color fundus photography (CFP) (Visucam Pro NM; Carl Zeiss Meditec AG, Jena, Germany), blue fundus autofluorescence,

and SD-OCT scanning. Optical coherence tomography scans were acquired using a Spectralis unit (Heidelberg Retina Angiograph [HRA]+OCT, Heidelberg Engineering, Heidelberg, Germany). Scan protocols included 37-line raster scans (20° × 15°) consisting of 512 A-scans for every line. Automated real-time function was turned on, and nine frames were acquired for each B-scan. The "follow-up" mode of the eye-tracking–assisted system (AutoRescan; Heidelberg Spectralis) was used at follow-up visits.

Fluorescein angiography (FA) and indocyanine green angiography (ICGA) were performed unless clinically contra-indicated. Fluorescein angiography and ICGA were performed using confocal scanning laser ophthalmoscopy (cSLO, HRA, Heidelberg Engineering). Our protocols involve an initial 20 seconds of video followed by stereoscopic imaging of both eyes at specific time points for up to 10 minutes for both eyes. Additional OCT scans are also acquired simultaneously, allowing point-to-point comparison of OCT along with FA and ICGA images.

For those patients with n-AMD who were deemed eligible to receive treatment, a loading phase of monthly intravitreal anti-VEGF injections, ranibizumab (0.5 mg per 0.05 mL) or aflibercept (2.0 mg per 0.05 mL), over a 3-month period was performed. After patients received the loading dose, they were retreated with ranibizumab as needed on the basis of evidence of new retinal hemorrhage, recurrence or persistence of intra- or subretinal fluid on OCT scans, or loss of visual acuity of more than 5 ETDRS letters without onset of foveal atrophy. After patients completed the loading phase, a fixed regimen of bimonthly injections was followed for the patients receiving aflibercept.

After excluding other diagnoses, we selected the first 117 consecutive patients with confirmed n-AMD who were eligible for inclusion. For eligibility, we specified the following criteria: commencement using anti-VEGF treatment and follow-up of at least 12 months, imaging by CFP, FA, ICGA, and OCT at baseline and OCT at visits 1, 3, and 12, and finding of less than

TABLE 2. Proportion of Eyes Presenting Changes in Morphology of Hyperreflective Material After Anti-VEGF Treatment by CNV Subtype

CNV	Baseline		Month 1		Month 3		Month 12	
	W-def	Undef	W-def	Undef	W-def	Undef	W-def	Undef
Type 1, *n* = 40	37.5%, 15/40	35.0%, 14/40	40.0%, 16/40	7.5%, 3/40	37.5%, 15/40	7.5%, 3/40	42.5%, 17/40	5.0%, 2/40
Type 2, *n* = 24	25.0%, 6/24	70.8%, 17/24	83.3%, 20/24	8.3%, 2/24	87.5%, 21/24	8.3%, 2/24	79.2%, 19/24	12.5%, 3/24
Type 3, *n* = 30	16.7%, 5/30	70.0%, 21/30	40.0%, 12/30	3.3%, 1/30	30.0%, 9/30	0.0%, 0/30	23.3%, 7/30	6.7%, 2/30
Mixed, *n* = 15	40.0%, 6/15	60.0%, 9/15	66.7%, 10/15	13.3%, 2/15	53.3%, 8/15	20.0%, 3/15	46.7%, 7/15	6.7%, 1/15
PCV, *n* = 12	58.3%, 7/12	33.3%, 4/12	50.0%, 6/12	33.3%, 4/12	33.3%, 4/12	8.3%, 1/12	41.7%, 5/12	8.3%, 1/12
Total, *n* = 121	32.2%, 39/121	53.7%, 65/121	52.9%, 64/121	9.9%, 12/121	47.1%, 57/121	7.4%, 9/121	45.5%, 55/121	7.4%, 9/121

CNV, choroidal neovascularization; W-def, well defined; Undef, undefined. The fractionated values refer to the relative frequency of the hyper-reflective material morphology in the different neovascular subtypes.

TABLE 3. Proportion of Eyes Presenting Changes in Location of HRM After Anti-VEGF Therapy by CNV Subtype

CNV	Baseline			Month 1			Month 3			Month 12		
	SR	SR&IR	subRPE	SR	SR&IR	subRPE	SR	SR&IR	subRPE	SR	SR&IR	subRPE
Type 1, n = 40	70.0%, 28/40	2.5%, 1/40	0.0%, 0/40	37.5%, 15/40	0.0%, 0/40	10.0%, 4/40	30.0%, 12/40	0.0%, 0/40	15.0%, 6/40	17.5%, 7/40	0.0%, 0/40	30.0%, 12/40
Type 2, n = 24	95.8%, 23/24	0.0%, 0/24	0.0%, 0/24	45.8%, 11/24	0.0%, 0/24	45.8%, 11/24	41.7%, 10/24	0.0%, 0/24	54.2%, 13/24	29.2%, 7/24	0.0%, 0/24	62.5%, 15/24
Type 3, n = 30	36.7%, 11/30	46.7%, 14/30	3.3%, 1/30	33.3%, 10/30	0.0%, 0/30	10.0%, 3/30	20.0%, 6/30	0.0%, 0/30	10.0%, 3/30	25.0%, 6/30	3.3%, 1/30	6.7%, 2/30
Mixed, n = 15	93.3%, 14/15	6.7%, 1/15	0.0%, 0/15	53.3%, 8/15	6.7%, 1/15	20.0%, 3/15	46.7%, 7/15	6.7%, 1/15	20.0%, 3/15	13.3%, 2/15	0.0%, 0/15	40.0%, 6/15
PCV, n = 12	83.3%, 10/12	8.3%, 1/12	0.0%, 0/12	75.0%, 9/12	8.3%, 1/12	0.0%, 0/12	33.3%, 4/12	0.0%, 0/12	8.3%, 1/12	33.3%, 4/12	0.0%, 0/12	16.7%, 2/12
Total, N = 121	71.1%, 86/121	14.0%, 17/121	0.8%, 1/121	43.8%, 53/121	1.7%, 2/121	17.3%, 21/121	32.2%, 39/121	0.8%, 1/121	21.5%, 26/121	21.5%, 26/121	0.8%, 1/121	30.6%, 37/121

CNV, choroidal neovascularization; SR, subretinal; SR&IR, sub- and intraretinal; subRPE, subretinal pigment epithelial. The fractionated values refer to the relative frequency of the hyper-reflective material location in the different neovascular subtypes.

TABLE 4. Proportion of Eyes With Exudative Manifestation by OCT Tissue Compartment Before and After Anti-VEGF Treatment

Characteristic	Baseline	Month 1	Month 3	Month 12
PED				
Fibrovascular	28.1%	23.1%	19.8%	19.1%
Serous	10.7%	7.4%	5.8%	5.0%
RPEE	31.4%	28.1%	29.8%	28.1%
Total	70.2%	58.7%	55.3%	52.1%
SRF	79.3%	36.4%	29.8%	32.2%
IRF	45.5%	18.2%	22.3%	30.6%

IRF, intraretinal fluid; PED, pigment epithelial detachment; RPEE, irregular shallow retinal pigment epithelial elevation; SRF, subretinal fluid.

75% fibrosis of the neovascular lesion at treatment initiation. There were no VA eligibility criteria.

Grading

We graded the image sets from baseline and OCT images at 4 time points, including baseline and months 1, 3, and 12 after initiation of anti-VEGF treatment. Color images from baseline and month-12 visits were graded for presence of blood, lipid, and fibrin without scrutinizing accompanying OCT scans. Fluorescein angiography and ICGA images were graded to determine the type of n-AMD, using the definitions provided by a recent classification,[15] after which the eyes were classified as occult (type 1), classic (type 2), retinal angiomatous proliferative (type 3), or polypoidal choroidal vasculopathic (PCV).

We used the recently developed consensus of definitions of OCT nomenclature.[16] The RPE was defined as the hyperreflective band between the choriocapillaris and the interdigitation zone (this band is not normally separable

TABLE 5. BCVA at Baseline and Month 12 by Category of Disruption of the Outer Retinal Bands Graded on OCT

Location	Proportion Disrupted at Baseline	Initial BCVA	Proportion Disrupted at M-12	M-12 BCVA
RPE				
Intact	18.2%	67.5	46.3%	68.2
25% disrupted	38.8%	59.7	38.0%	62.6
50% disrupted	28.1%	57.9	9.1%	63.4
75% disrupted	13.2%	56.8	6.6%	47.6
100% disrupted	1.7%	45.5	0.0%	NA
EZ				
Intact	1.7%	52.0	4.1%	64.0
25% disrupted	0.8%	59.0	13.2%	73.1
50% disrupted	10.7%	70.9	19.0%	69.3
75% disrupted	13.2%	61.3	28.1%	62.6
100% disrupted	73.6%	58.3	35.5%	59.7
ELM				
Intact	4.1%	64.4	23.1%	72.0
25% disrupted	14.0%	69.1	39.7%	66.8
50% disrupted	22.3%	61.3	18.2%	55.9
75% disrupted	31.4%	61.1	15.7%	58.8
100% disrupted	28.1%	52.4	3.3%	53.3

BCVA, best-corrected visual acuity; ELM, external limiting membrane; EZ, ellipsoid zone; M-12, month 12; RPE, retinal pigment epithelium.

TABLE 6. Difference in Mean BCVA at Month 12 by Presence and Morphology of HRM at Month 12

HRM	Mean ± SD BCVA at M-12	Significance	95% Confidence Interval
No HRM, $n = 54$	66.3 ± 14.0	Reference group	
W-def HRM, $n = 58$	63.3 ± 16.2	0.29	−2.6 to 8.7
Undef HRM, $n = 9$	59.1 ± 10.4	0.09	−1.3 to 15.7

BCVA, best-corrected visual acuity; HRM, hyperreflective material; W-def, well defined; Undef, undefined.

from Bruch's membrane in the scans from current generation of SD-OCT scans and is therefore referred to as RPE/Bruch's complex). The EZ was defined as the second hyperreflective band internal to the RPE. The ELM was defined as a discrete hyperreflective band at the outermost border of the outer nuclear layer and located internal to the EZ band. We examined all scans of the macular raster for regions of abnormal hyperreflectivity and localized these to intraretinal (IR), subretinal, and subretinal pigment epithelial (sub-RPE) compartments. We used the definitions described by Ores et al.[17] to distinguish between types of HRM. Hyperreflective material with high reflectivity, whose

TABLE 7. Variables Influencing BCVA on Multivariate Regression Analysis

Dependent Variable	Predictor(s) Selected	B	t	Significance
Baseline BCVA	ELM disruption at baseline	−4.05	−4.30	<0.001
	Age	−0.37	−2.76	0.007
	PED present at baseline	5.94	2.53	0.010
Month 12 BCVA	ELM disruption at baseline	−3.67	−3.32	0.001
	Age	−0.33	−2.06	0.042
	Number of treatments	1.38	2.04	0.041
Month 12 BCVA	ELM disruption at M-12	−5.14	−4.60	<0.001
	SRF present at M-12	7.26	2.77	0.007
Change in BCVA	ELM disruption at M-12	−3.58	−4.16	<0.001
	CNV subtype	1.80	2.51	0.013
	Number of treatments	1.09	2.17	0.032

B, Beta coefficient; BCVA, best-corrected visual acuity; CNV, choroidal neovascularization; ELM, external limiting membrane; PED, pigment epithelial detachment; SRF, subretinal fluid; t, t statistic.
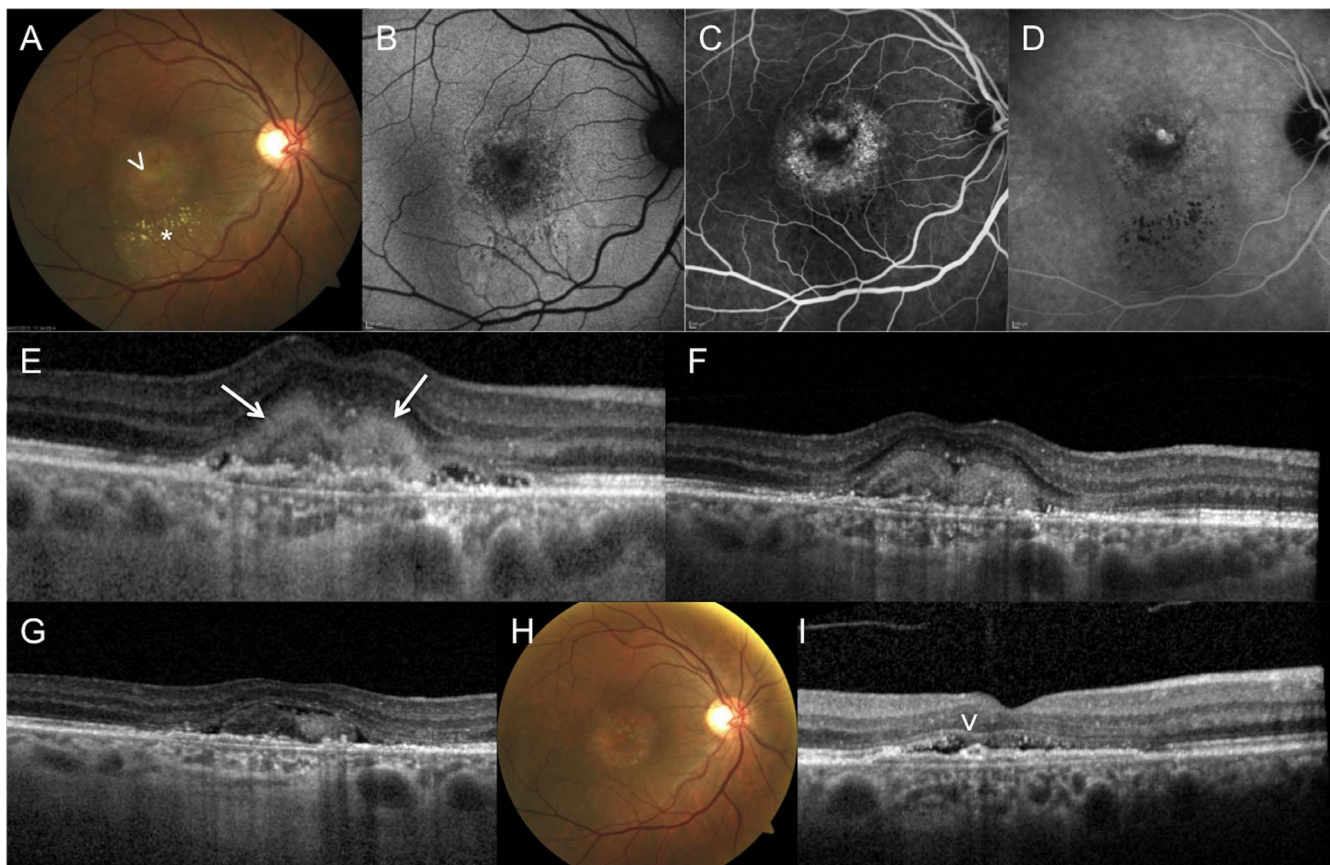

FIGURE 1. Multimodal imaging of neovascular AMD of the right eye. Best-corrected visual acuity at presentation was 53 ETDRS letters. (*Upper panel*) Baseline images include the color fundus photograph (CFP) (**A**), blue autofluorescence (**B**), representative frames of the fluorescein angiogram (**C**), and indocyanine green angiogram (**D**). Color fundus photograph (**A**) reveals fibrin (*arrowhead*) and accumulation of lipids (*asterisk*). On FA (1 minute 42 seconds) the selected frame shows speckled hyperfluorescence, and on ICGA (8 minutes 49 seconds) there is a "hot spot" (confirming a type 1 CNV). The corresponding baseline OCT scan (**E**) shows shallow elevation of the retinal pigment epithelium and subretinal hyperreflective material with undefined boundaries and disruption of the ellipsoid zone and partial disruption of external limiting membrane. Subsequent OCT scans at 1 month (**F**) show disappearance of the fuzzy border. By 3 months (**G**), the subretinal HRM has reduced, and the boundaries become well defined. By month 12 (**I**), resolution of HRM with complete restoration of ELM (*arrowhead*) is seen. Color fundus photograph at month 12 (**H**) shows resolution of fibrin and lipid deposition. Final BCVA is 50 ETDRS letters.
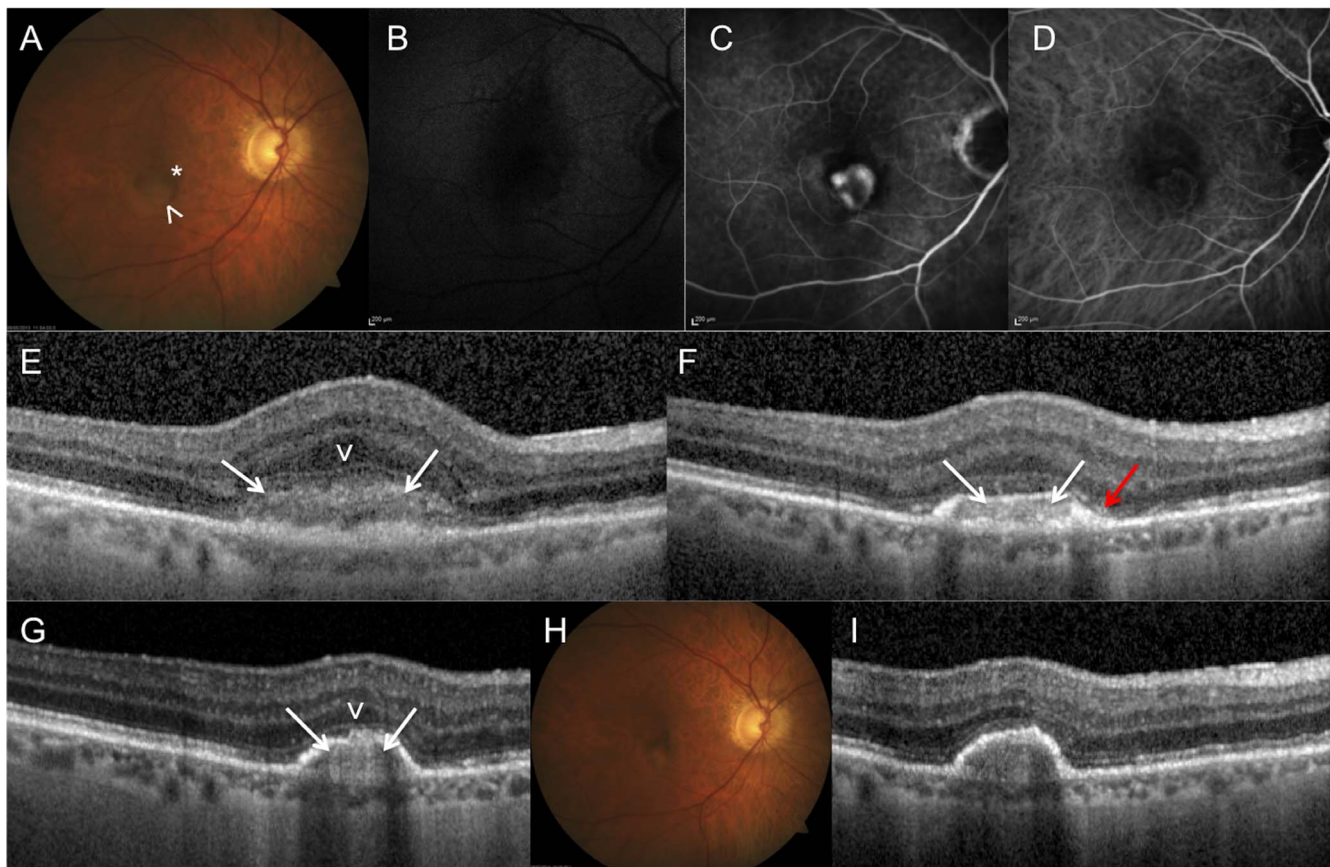
FIGURE 2. Multimodal imaging of neovascular AMD of the right eye. Best-corrected visual acuity at presentation is 45 ETDRS letters. Images from the baseline visit are shown in the top panel. Color fundus photograph (**A**) shows fibrin (*arrowhead*) and perilesional hemorrhage (*asterisk*). Fluorescein angiography frame (40 seconds) shows an area of well defined hyperfluorescence, and the corresponding ICGA (1 minute 45 seconds) shows a neovascular net (confirming a type 2 CNV). Baseline OCT scans (**E**) reveal subretinal HRM with undefined boundaries (*arrows*) and an almost intact ELM (*arrowhead*). Subsequent OCT scans showed that, at 1 month (**F**), subretinal HRM has resolved. New HRM is present in the sub-RPE space (*arrows*). New HRM boundaries are well defined. At 3 (**G**) and 12 (**I**) months there is persistent sub-RPE HRM with well-defined boundaries and complete restoration of ELM (*arrowhead*). Note the splitting of the RPE without any overlying HRM at month 1 (*red arrow*). Color fundus photograph at month 12 (**H**) shows a pigmented inactive CNV with neither fibrin nor perilesional hemorrhage. Final BCVA was 76 ETDRS letters.

boundaries could be clearly delineated from the surrounding neural components of the retina, were classified as well defined. Hyperreflective material with low reflectivity and whose borders were less well distinguishable from surrounding neural components were classified as undefined.

Optical coherence tomography scans were also graded for the presence of pigment epithelium detachment (PED), subretinal fluid (SRF), cystic intraretinal fluid (IRF), integrity of the outer retinal layers of the RPE, EZ, and ELM. Pigment epithelial detachment was graded as fibrovascular, serous, or irregular shallow retinal pigment epithelium elevation. The scan with the maximum pathology was selected for grading of RPE, EZ, and ELM layer integrity. A graded categorical approach was used to determine intactness of these layers, with a score of 0, which indicated an intact layer; 1, 25% disrupted layer; 2, 50% disrupted layer; 3, 75% disrupted layer; and 4, completely disrupted layer.

Grading was performed by a single retina specialist (G.C.) with quality assurance carried out by two retina specialists (U.C. and F.B.).

Statistical Analysis

Data were analyzed using SPSS version 21 software (SPSS; IBM, Armonk, NY, USA). Descriptive statistics were generated for continuous variables and categorical variables. Hyperreflective material presence and location graded on OCT scans were correlated with lesion components present in color images and with lesion subtype graded using angiography. Pearson's correlation coefficients were used to examine for associations between variables graded using CFP and those using OCT. Cross-tabulations were performed to test associations between HRM type and CFP variables and χ^2 tests used to examine for significant associations. Multivariate regression analysis with forward selection was used to generate models to examine the effects of baseline patient characteristics and morphologic variables measured at baseline and final visit on function. To do this, we ran a series of models. In model 1, the dependent variable was baseline BCVA, and the explanatory variables included age, sex, CNV subtype, and OCT morphologic measurements made at the baseline visit. In model 2, we retained the same explanatory variables as in model 1 along with the number of treatments given and regressed these against the final BCVA, which was entered as the dependent variable. In model 3, we included age, sex, CNV subtype from baseline, number of treatments given, and morphologic characteristics at the final visit, which were regressed against final BCVA. In model 4, we entered the change in BCVA as the dependent variable, and we regressed this against age, sex, number of treatments given, and morphologic variables measured at the final visit.
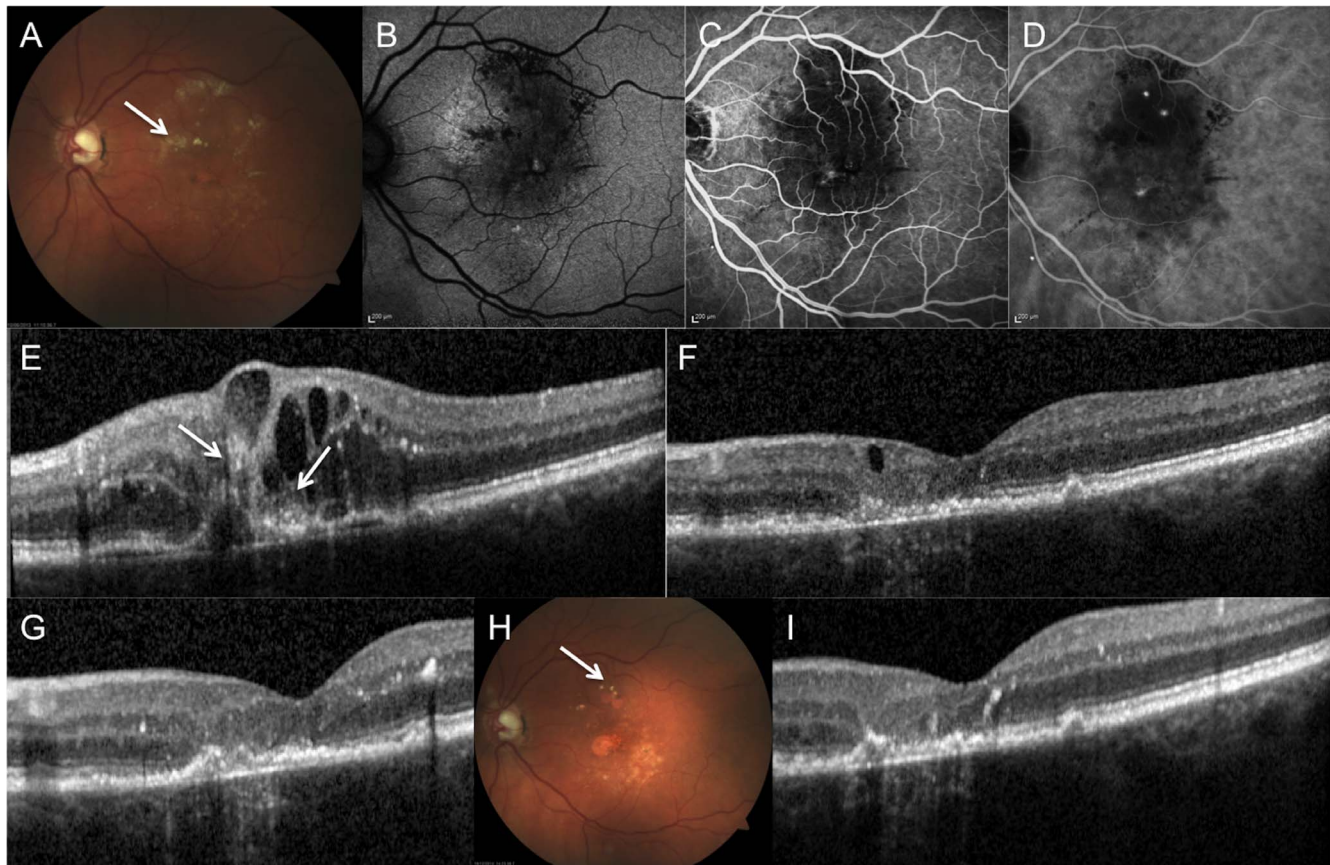
FIGURE 3. Multimodal imaging of neovascular AMD of the left eye. Best-corrected visual acuity at presentation was 45 ETDRS letters. Color fundus photograph (**A**) shows extensive lipid accumulation (*arrow*). Fluorescein angiography (**C**) and ICGA (**D**) show "hot spots" consistent with multifocal type 3 CNV. Baseline OCT scans show (**E**) sub- and intraretinal HRM with undefined boundaries (*arrows*) and disruption of RPE, EZ, and ELM. Subsequent scans at 1 month (**F**) shows complete resolution of sub- and intraretinal HRM with partial recovery of the RPE, EZ, and ELM. Retinal pigment epithelium and EZ layers show further signs of recovery at 3 (**G**) and 12 (**I**) months, but the ELM remains disrupted. Color fundus photograph at month 12 (**H**) shows RPE atrophy and resolving lipid deposition (*arrow*). Final BCVA was 56 ETDRS letters.

RESULTS

Baseline Characteristics

Baseline characteristics of the 121 eyes with active n-AMD (40 type 1, 24 type 2, 30 type 3, 15 mixed, and 12 PCV) from 117 patients are summarized in Table 1. The mean age of the sample population was 77.5 (range, 53–97) years, and 74 were females. Mean BCVA improved after treatment, from 59.9 ± 13.24 at baseline to 64.3 ± 14.9 ETDRS letters at month 12. The mean number of intravitreal injections performed during year 1 was 7.38 ± 1.89 (range, 3–11). A total of 113 eyes received ranibizumab, of which 9 with PCV underwent a combination treatment with verteporfin photodynamic therapy. Eight eyes were treated with aflibercept. No statistically significant differences were observed among the CNV subtype groups for the number of intravitreal injections administered.

Color image grading showed that blood and fibrin were visible in approximately half of all eyes and that lipid exudates were present in approximately one-fourth (Table 1). Blood was present in almost all eyes presenting with PCV (91.7%, 11 of 12 eyes) and in a significant proportion of eyes presenting with type 3 CNV (76.7%, 23 of 30 eyes).

On OCT grading HRM was found to be present in 85.9% (104 of 121) of eyes at the baseline visit. The morphology of HRM is shown in Table 2. Hyperreflective material was present in all CNV subtypes but was most commonly encountered in type 2 and mixed CNV. In more than half of the eyes (53.7%, 65 of 121), HRM had undefined boundaries, and this morphology was observed most frequently in types 2 and 3 CNV compared to the other CNV types. The location of HRM is shown in Table 3. At baseline, approximately three-quarters of eyes had HRM in the subretinal compartment only. Hyperreflective material was also seen in the intraretinal compartment in 17 eyes (14.0%), of which 14 had a retinal angiomatous proliferative lesion. Hyperreflective material was uncommon in the sub-RPE compartment.

Correlation coefficients showed that HRM presence was most strongly associated with fibrin on CFP ($r = 0.57$; $P < 0.001$). Cross-tabulation between presence of fibrin and HRM type revealed ($\chi^2 = 39.87$; $P < 0.001$) the association was strongest with the undefined type. In 6 eyes, HRM was the only OCT feature indicating n-AMD lesion activity, and of these, 5 showed a retinal hemorrhage on CFP.

Morphologic Changes After Treatment

At month 12, the overall prevalence of fibrin, blood, and lipid on CFPs was markedly reduced (Table 1). Presence of blood resolved in all but one of the eyes with PCV and was found to be still present in a small proportion of type 3 CNV eyes.

The overall prevalence of HRM fell from 85.9% at baseline to 52.9% by month 12, along with substantial differences in terms of morphology and location over time (Tables 2, 3). Undefined
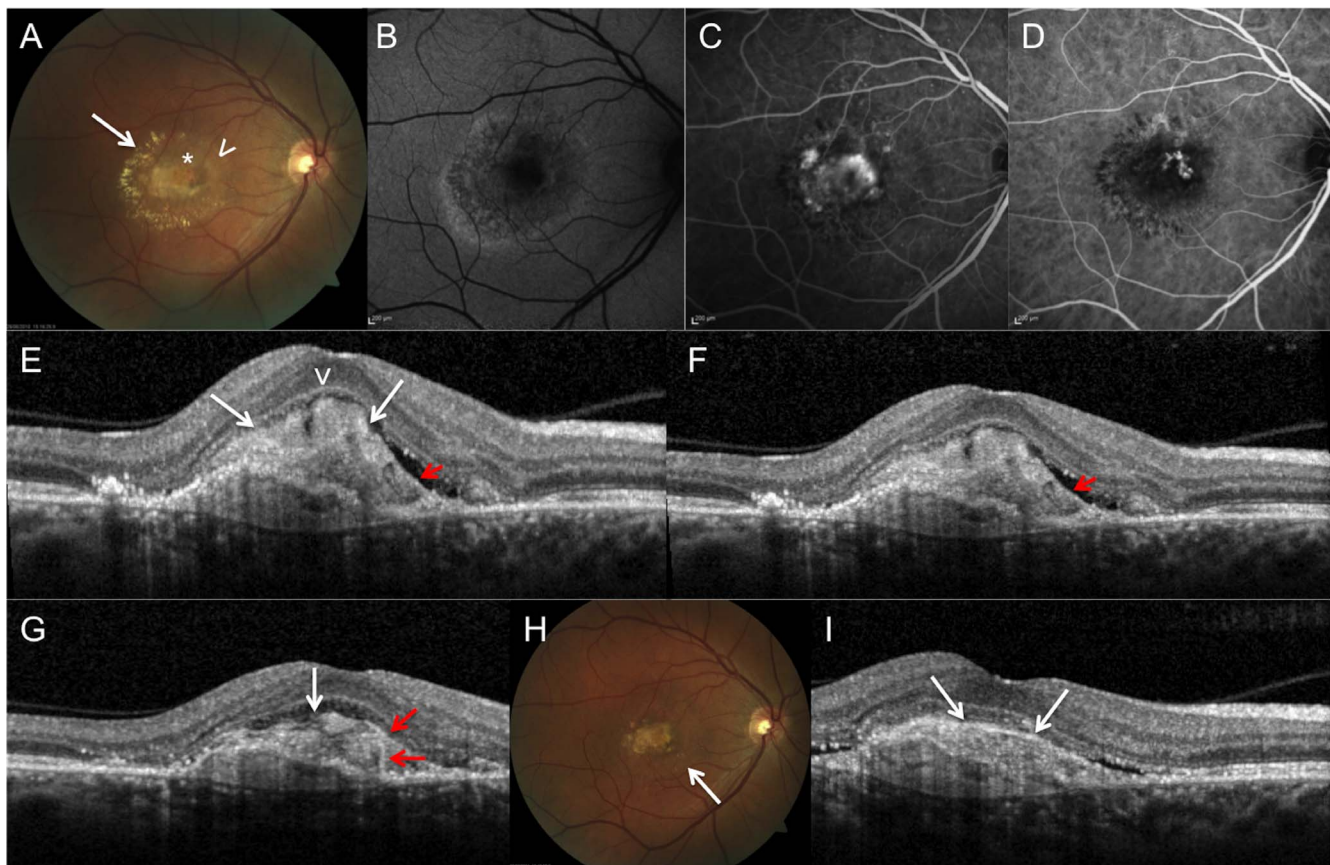
FIGURE 4. Multimodal imaging of neovascular AMD of the right eye. Best-corrected visual acuity at presentation was 53 ETDRS letters. Color fundus photograph (**A**) shows fibrin (*arrowhead*), small dot blot retinal hemorrhages (*asterisk*), and lipid accumulation (*arrow*). The FA (**C**) shows marked early hyperfluorescence, and the ICGA (**D**) shows the profiles of polypoidal lesions within a branching vascular network and confirms the diagnosis of polypoidal choroidal vasculopathy (PCV). Baseline OCT scans (**E**) show subretinal HRM with well-defined boundaries (*arrows*) and an almost intact ELM (*arrowhead*) with partial disruption of the RPE. Subsequent scans at 1 month (**F**) and at 3 months (**G**) show reduced subretinal HRM and complete resolution at month 12 (**I**). However, sub-RPE HRM is present at month 12 (*arrows*). The splitting of the RPE, which consolidates over time, is noted from the baseline scans (*red arrows*). Color fundus photograph at month 12 (**H**) shows a fibrotic scar with resolving lipid deposition (*arrow*). Final BCVA was 70 ETDRS letters.

HRM was dramatically reduced from 53.7% at baseline to 7.4% at month 12, with the most obvious reduction occurring within 1 month. By contrast, areas of well-defined HRM appeared over time, and the overall proportion increased from 32.2% at baseline to 45.5% at month 12. Subretinal HRM steadily reduced from baseline (71.1%) to month 12 (21.5%). In contrast, sub-RPE HRM, which was infrequent at baseline, increased up to 30.6% by month 12. Differences were observed in the evolution of HRM in the various CNV subtypes. In type 1 CNV, although the frequency of undefined HRM reduced over time, well-defined HRM did not change markedly. In type 2 CNV, undefined HRM was reduced within 1 month of treatment, but well-defined HRM increased so that the overall frequency remained the same. In type 3, undefined HRM was dramatically reduced within 1 month, and the overall prevalence of HRM was reduced over time. A decrease in the prevalence of well-defined HRM was observed only in the PCV group. The sub-RPE HRM was more frequently observed in type 2 CNVs.

The frequency at which PED, SRF, and IRF were observed on OCT scans at baseline and at subsequent visits is shown in Table 4. Fibrovascular and serous PEDs decreased in frequency over time, but shallow, irregular elevation of the RPE did not change. Marked reductions in sub- and intraretinal fluid were observed within 1 month, but the proportion of eyes with IRF rose from a low of 18.2% at month 1 to 30.6% at month 12.

Relationships Between BCVA and OCT Parameters

The presence of HRM was associated with poorer baseline BCVA than with eyes without HRM. On univariate analysis, the patient's age, presence of fibrin, blood, SRF, and IRF on OCT scans, disruption of outer retinal bands, and CNV subtype had statistically significant influences on baseline BCVA. The proportions of eyes grouped by severity of disruption of RPE, EZ, and ELM at baseline and month 12 are shown in Table 5. Improvements in intactness of the RPE, EZ, and ELM were seen with mean BCVA best in eyes with least disruption and worst in eyes with maximum disruption. At month 12, the BCVA gradient was best appreciated in the graded categories of ELM intactness ranging from 72.0 ETDRS letters in eyes with intact ELM to 53.3 letters in the most disrupted group.

A gradation of BCVA was observed with the best VA outcome at month 12 in the absence of any HRM, the worst with undefined HRM, and midway for well-defined HRM (Table 6).

Table 7 summarizes the results from the four models. In model 1, ELM intactness, age, and presence of PED were
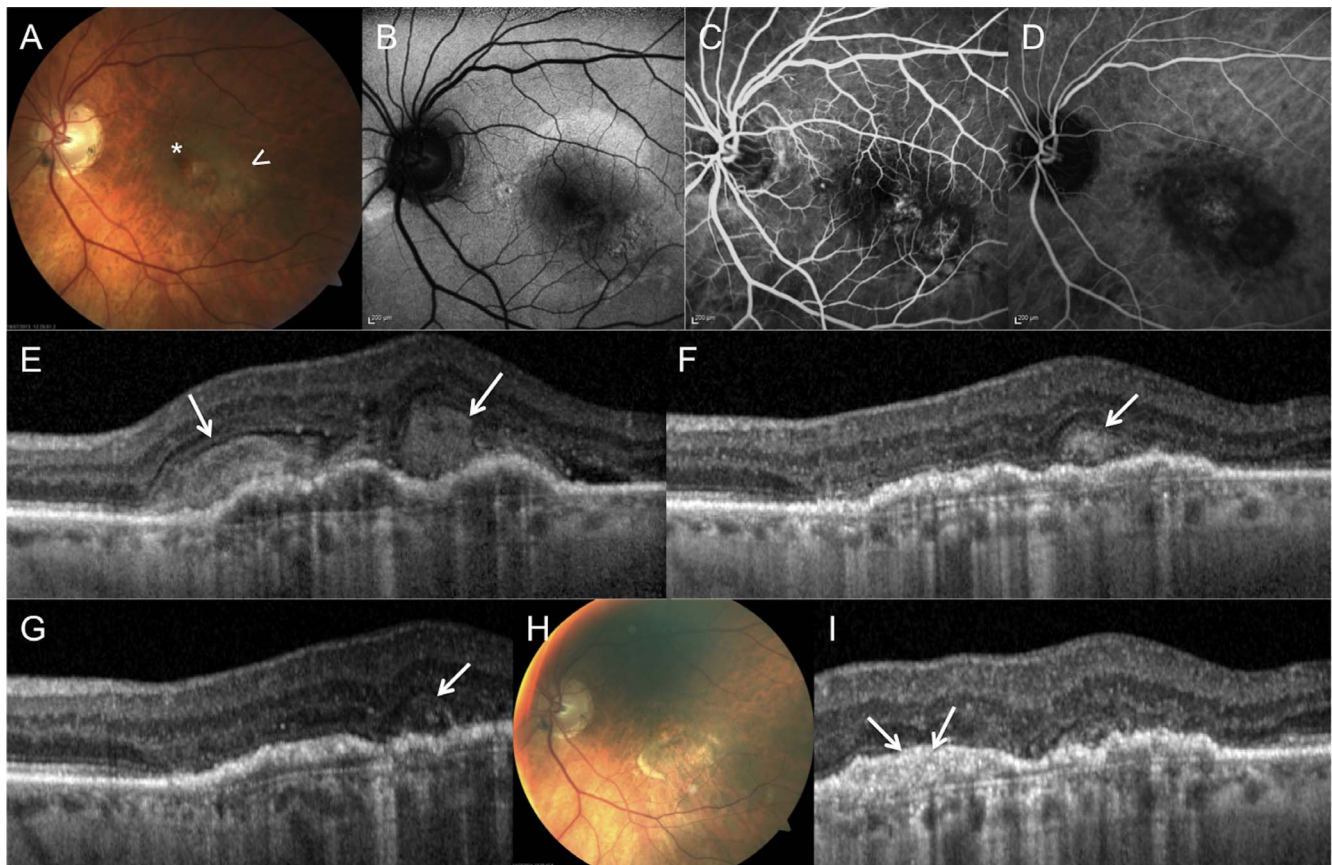
FIGURE 5. Multimodal imaging of neovascular AMD of the left eye. Best-corrected visual acuity at presentation was 30 ETDRS letters. Color fundus photograph (**A**) shows fibrin (*arrowhead*) and perilesional hemorrhage (*asterisk*). Fluorescein angiography frame (42 seconds) (**C**) shows speckled hyperfluorescence, and the ICGA (**D**) reveals a diffuse staining plaque (11 minute 2 seconds). Baseline OCT scans (**E**) show subretinal HRM with well-defined boundaries (*arrows*). At subsequent visits there was reduced subretinal HRM (*arrow*) at month 1 (**F**), and by month 3 (**G**), there was only minimal HRM (*arrow*). Hyperreflective material in the subretinal space was resolved by month 12 (**I**), and sub-RPE HRM with well-defined boundaries (*arrows*) was seen at that visit. Color fundus photograph at month 12 (**H**) shows a mild fibrotic scar and RPE atrophy. Final BCVA was 35 ETDRS letters.

included whereas all other variables including HRM were omitted from the model. On replacing the 12-month BCVA as the dependent variable and including number of treatments in the independent list, ELM intactness at baseline, age, and number of treatments were incorporated in model 2, and all other variables were excluded. In model 3, which also retained 12-month BCVA as the dependent variable but where the independent variables included were OCT morphologic measurements made at month 12, the forward selection algorithm retained only ELM disruption, and presence of SRF. External limiting membrane disruption had a negative effect on BCVA, whereas the presence of SRF at month 12 had a positive effect. Model 4, with change in BCVA as the dependent variable, showed that ELM disruption at month 12, number of treatments, and baseline CNV subtype were statistically significant predictors and were included in the model. For each level of severity of ELM disruption BCVA was approximately 3.6 letters worse, whereas positive predictors were CNV subtype and number of treatments.

DISCUSSION

There has been a growing interest in the component termed SHRM, observed on OCT scanning in n-AMD. Various investigators have reported that SHRM occurs on fluorescein angiograms of eyes with leakage activity,[10,11] but that it may also correlate with hemorrhage, lipid, or thick fibrin.[18]

Recently, various studies have described the presence of SHRM in treatment-naive n-AMD.[17,19] Sha et al.[19] used the term "subretinal hyperreflective exudation" to describe a form of SHRM different from hemorrhage, lipid, subretinal fibrosis, and neovascular process itself; they noted that this distinct form of SHRM may be the only sign of early active n-AMD and that it promptly resolves following anti-VEGF treatment. Ores et al.[17] also described the same OCT finding as "gray hyperreflective subretinal lesion," suggesting that its presence is an early sign of n-AMD. It has been speculated that this material is exudative in nature and most probably composed of fibrin as a result of the inflammatory reaction concomitant to the neovascular process.[19]

In the present study, we undertook a systematic multimodal imaging analysis of HRM with correlations to CFP and angiographic subtypes. We prefer to use the term "hyperreflective material" because our data show that HRM can also have an intraretinal location, especially in type 3 CNVs. In our dataset, HRM was a frequent OCT finding among all CNV subtypes; however, the presence of HRM as the only OCT sign of CNV activity in treatment naive eyes was infrequent (4.9%, 6/121).

We observed a strong correlation between presence of fibrin on CFP and presence of HRM on OCT before initiation of
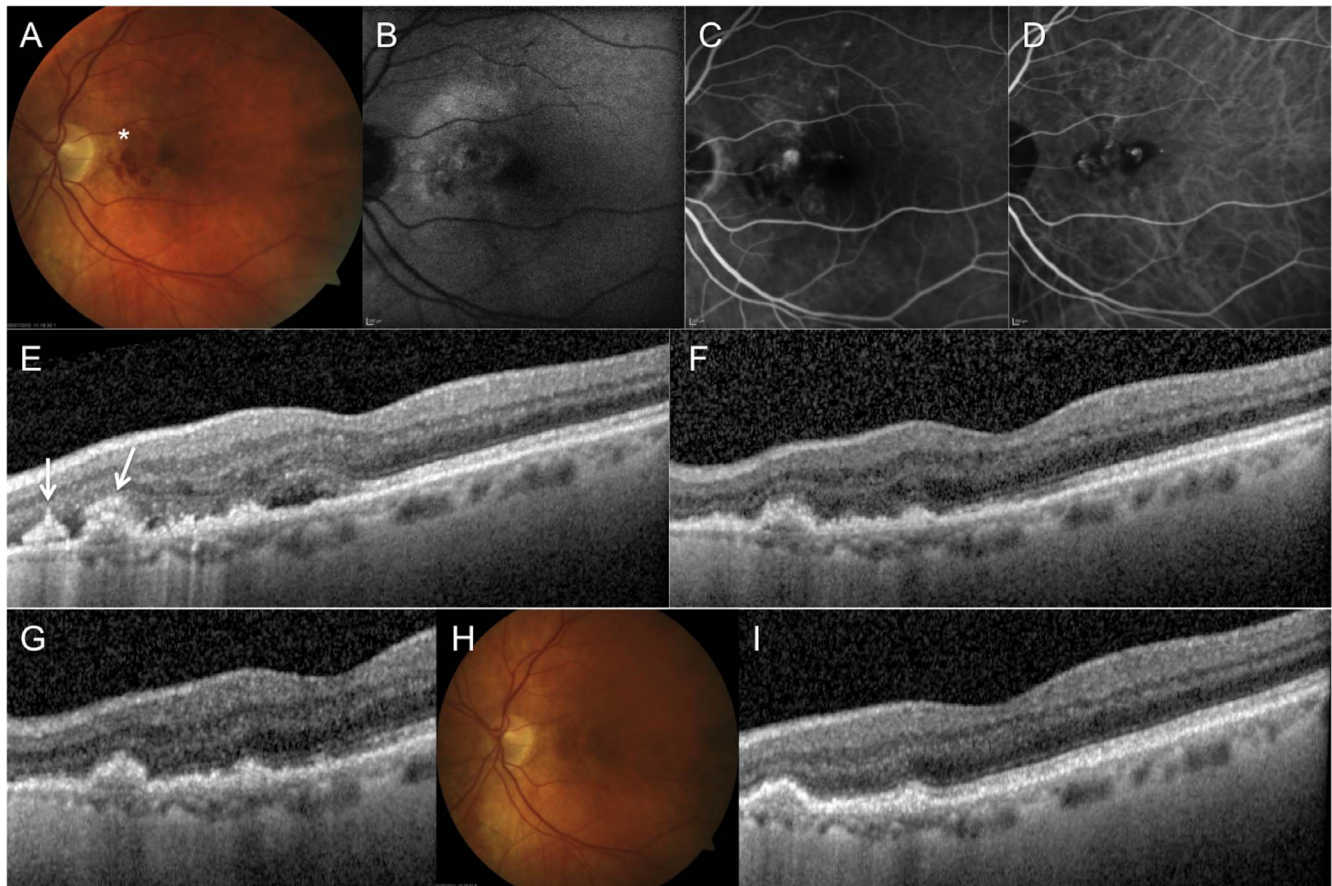
FIGURE 6. Multimodal imaging of neovascular AMD of the left eye. Best-corrected visual acuity at presentation was 59 ETDRS letters. Color fundus photograph (**A**) shows retinal hemorrhage (*asterisk*). Fluorescein angiography (**C**) shows late hyperfluorescence, whereas ICGA (**D**) shows polypoidal profiles with branching vascular network, confirming the diagnosis of PCV. Baseline OCT scans (**E**) show subretinal fluid with a localized well-defined HRM (*arrows*). Subsequent scans at 1 month (**F**) show resolving HRM, which appears to be completely resolved by 3 months (**G**) and 12 months (**I**) after initiation of treatment. Color fundus photograph at month 12 (**H**) shows complete resorption of the retinal hemorrhage. Final BCVA was 69 ETDRS letters.

anti-VEGF therapy. This finding along with the marked reduction in the undefined component of HRM by month 1 suggests that the subset of HRM that is diffuse and located in the subretinal space is the result of an inflammatory reaction in early n-AMD. We also observed the increase of HRM with well-defined boundaries over time and that undefined HRM was frequently replaced by the well-defined variety after anti-VEGF therapy. This supports the observation that anti-VEGF treatment induces a maturation of the neovascular complexes towards an organized tissue in which hyperreflectivity increases over time. In agreement with the latter observation, Charafeddin et al.[20] have recently shown that reduction of thickness and volume of SHRM is accompanied by increase of the mean reflectivity following anti-VEGF treatment. However, the exact composition of this tissue remains a matter of speculation and others have hypothesized that it may reflect higher concentrations of inflammatory cells[17] and/or fibrotic elements.[11,20]

In our series, we observed a decrease in subretinal well-defined HRM over time in the PCV group. In the PCV group, the color grading outputs indicated the presence of hemorrhage at baseline, which explained the presence of well-defined HRM. Resorption of blood following anti-VEGF therapy was accompanied by the resolution of well-defined HRM.

Because we had morphologic descriptors measured at both baseline and final visit, we ran a series of models to examine the temporal relationships between function and morphology. In our first model, we showed that baseline BCVA is best explained by ELM intactness, with age and PED presence contributing minimally to the model. Similarly, ELM intactness remained the most consistent variable that explained most of the variations in BCVA outcome. A strong relationship was noted between the ELM severity of disruption and visual acuity both in the cross-sectional associations at baseline and month 12 and in terms of explaining the change in BCVA.

With respect to HRM, our models did not select for this morphologic parameter as an important contributor to either baseline or final BCVA. However, we did observe that eyes with no HRM at month 12 had best mean VA, those with undefined HRM had the worst mean VA, and those with well-defined HRM falling between these two categories. Our data support the recent subanalysis of the CATT study,[13] where persistent SHRM was associated with worse visual acuity outcomes along with a higher incidence of scarring when compared with eyes without SHRM.

The finding that eyes with undefined HRM at month 12 had the poorest vision suggests a reactivation of the CNV complex and supports the recommendation by Ores et al. to consider undefined HRM as a qualitative criterion for retreatment.[17]

Of note, in our study, sub-RPE location of HRM was almost exclusively observed following anti-VEGF treatment. The sub-RPE location was also more frequently observed in type 2 CNVs. We therefore speculate that subretinal HRM and sub-RPE HRM reflect two different pathologic processes. We hypothesize that the sub-RPE location of HRM arises as a consequence of reactive hyperplasia of the RPE which proliferates enclosing the subretinal HRM in the post treatment phases (Figs. 2 and 4). This finding has been described to occur following anti-VEGF treatment in myopic CNVs,[21] which typically display type 2 CNV features.

Optical coherence tomography angiography (OCTA) has made it possible to noninvasively generate three-dimensional images of the retinal and choroidal vessels,[22] which show good specificity for detection of the CNV compared to FA.[23] The changes in the neovascular complex in the post treatment phases of antiangiogenic treatment have been imaged using OCTA and these studies have revealed a remodeling of the neovascular complex,[24] which seems to be more evident in the first two weeks after the administration of the intravitreal injection.[25,26] These studies have reported rapidity in the remodeling of the CNV network on OCTA, and are consistent with our observation of morphologic changes in HRM one month after treatment in our case series.

Current evidence suggests that the status of the OCT outer retinal bands are important predictors in determining the visual outcome of anti-VEGF treatment.[7–9] Recently Coscas et al.[9] showed that the visual outcome correlated with restoration of ELM, but not with the restoration of EZ. Our data confirm the latter results and support the evidence of ELM as an useful biomarker for visual acuity improvement at month 12.

In our study the presence of SRF at month 12 was associated with higher BCVA. This finding is intriguing and supports a growing evidence of a possible beneficial effect of SRF for the RPE and photoreceptor survival in patients with n-AMD.[7]

Strengths of our study are the multimodal imaging approach with high resolution OCT available for all included patients, the large sample size and characterization of CNV subtype and its inclusion in the analysis with follow up out to month 12.

We did not grade for fibrosis or atrophy and we did not make any quantitative measurements of the OCT characteristics and these are limitations of our study and thus we are unable to include these parameters of interest in our models. Also we only assessed the scan with the maximum pathology in detail and thus our measurements made on a single scan may not explain the changes in visual acuity of patients with extrafoveal location of pathology (such as the eyes of patients with PCV and type 3 CNV subtypes).

Among other limitations are those inherent in the resolution possible in the current generation of OCTs ability to detect anatomical structures in the context of neovascular disease. For instance, a shadow effect due to the presence of HRM on the outer retinal surface might have impaired the clarity of the underlying structures, including the RPE and sub-RPE HRM. Hence, HRM in the sub-RPE space may have been undetected and underestimated, particularly at baseline in our series.

In summary, in eyes with neovascular AMD, the location and morphology of HRM changed after anti-VEGF treatment. Before initiation of treatment, undefined HRM was commonly detected, notably in the subretinal location, and correlated with fibrin on CFP. After anti-VEGF treatment, most of the HRM observed had well-defined boundaries with increased reflectivity and was located in the sub-RPE space. Thus, the findings of the present study strongly support the view that this OCT feature represents fibrosed tissue and/or mature neovascular

complexes. Further studies will clarify whether well-defined HRM replaces the undefined HRM or whether the former develops de novo.

References

1. Klein R, Peto T, Bird A, Vannewkirk MR. The epidemiology of age-related macular degeneration. *Am J Ophthalmol*. 2004; 137:486–495.

2. Wong TY, Chakravarthy U, Klein R, et al. The natural history and prognosis of neovascular age-related macular degeneration: a systematic review of the literature and meta-analysis. *Ophthalmology*. 2008;115:116–126.

3. Solomon SD, Lindsley K, Vedula SS, Krzystolik MG, Hawkins BS. Anti-vascular endothelial growth factor for neovascular age-related macular degeneration. *Cochrane Database Syst Rev*. 2014;29; 8:CD005139.

4. Campbell JP, Bressler SB, Bressler NM. Impact of availability of anti-vascular endothelial growth factor therapy on visual impairment and blindness due to neovascular age-related macular degeneration. *Arch Ophthalmol*. 2012;130:794–795.

5. Hogg R, Curry E, Muldrew A, et al. Identification of lesion components that influence visual function in age related macular degeneration. *Br J Ophthalmol*. 2003;87:609–614.

6. Witkin AJ, Vuong LN, Srinivasan VJ, et al. High-speed ultrahigh resolution optical coherence tomography before and after ranibizumab for age-related macular degeneration. *Ophthalmology*. 2009;116:956–963.

7. Schmidt-Erfurth U, Waldstein SM. A paradigm shift in imaging biomarkers in the management of neovascular age-related macular degeneration. *Prog Retin Eye Res*. 2016;50:1–24.

8. Sayanagi K, Sharma S, Kaiser PK. Photoreceptor status after antivascular endothelial growth factor therapy in exudative age-related macular degeneration. *Br J Ophthalmol*. 2009;93: 622–626.

9. Coscas F, Coscas G, Lupidi M, Cagini C, Souied EH. Restoration of outer retinal layers after aflibercept therapy in exudative AMD: prognostic value. *Invest Ophthalmol Vis Sci*. 2015;56: 4129–4134.

10. Liakopoulos S, Ongchin S, Bansal A et al. Quantitative optical coherence tomography findings in various subtypes of neovascular age-related macular degeneration. *Invest Ophthalmol Vis Sci*. 2008;49:5048–5054.

11. Giani A, Esmaili DD, Luiselli C, et al. Displayed reflectivity of choroidal neovascular membranes by optical coherence tomography correlates with presence of leakage by fluorescein angiography. *Retina*. 2011;31:942–948.

12. Keane PA, Patel PJ, Liakopoulos S, Heussen FM, Sadda SR, Tufail A. Evaluation of age-related macular degeneration with optical coherence tomography. *Surv Ophthalmol*. 2012;57: 389–414.

13. Daniel E, Toth CA, Grunwald JE, et al. Risk of scar in the comparison of age-related macular degeneration treatments trials. *Ophthalmology*. 2014;121:656–666.

14. Willoughby AS, Ying GS, Toth CA, et al. Comparison of age-related macular degeneration treatments trials research group. subretinal hyperreflective material in the comparison of age-related macular degeneration treatments trials. *Ophthalmology*. 2015;122:1846–1853.

15. Freund KB, Zweifel SA, Engelbert MR. Do we need a new classification for choroidal neovascularization in age-related macular degeneration. *Retina*. 2010;30:1333–1349.

16. Staurenghi G, Sadda S, Chakravarthy U; for International Nomenclature for Optical Coherence Tomography (IN•OCT) Panel. Proposed lexicon for anatomic landmarks in normal posterior segment spectral-domain optical coherence tomography: the IN•OCT consensus. *Ophthalmology*. 2014;121: 1572–1578.

17. Ores R, Puche N, Querques G, et al. Gray hyper-reflective subretinal exudative lesions in exudative age-related macular degeneration. *Am J Ophthalmol*. 2014;158:354–361.

18. Joeres A, Tsong JW, Updike PG, et al. Reproducibility of quantitative optical coherence tomography subanalysis in neovascular age-related macular degeneration. *Invest Ophthalmol Vis Sci*. 2007;48:4300–4307.

19. Shah VP, Shah SA, Mrejen S, Freund KB. Subretinal hyper-reflective exudation associated with neovascular age-related macular degeneration. *Retina*. 2014;34:1281–1288.

20. Charafeddin W, Nittala MG, Oregon A, Sadda SR. Relationship between subretinal hyperreflective material reflectivity and volume in patients with neovascular age-related macular degeneration following anti-vascular endothelial growth factor treatment. *Ophthalmic Surg Lasers Imaging Retina*. 2015;46: 523–530.

21. Introini U, Casalino G, Querques G, Gimeno AT, Scotti F, Bandello F. Spectral-domain OCT in anti-VEGF treatment of myopic choroidal neovascularization. *Eye (Lond)*. 2012;26: 976–982.

22. Jia Y, Bailey ST, Wilson DJ, et al. Quantitative optical coherence tomography angiography of choroidal neovascularization in age-related macular degeneration. *Ophthalmology*. 2014;121: 1435–1444.

23. de Carlo TE, Bonini Filho MA, Chin AT, et al. Spectral-domain optical coherence tomography angiography of choroidal neovascularization. *Ophthalmology*. 2015;122:1228–1238.

24. Spaide RF. Optical coherence tomography angiography signs of vascular abnormalization with antiangiogenic therapy for choroidal neovascularization. *Am J Ophthalmol*. 2015;160:6–16.

25. Huang D, Jia Y, Rispoli M, Tan O, Lumbroso B. Optical coherence tomography angiography of time course of choroidal neovascularization in response to anti angiogenic treatment. *Retina*. 2015;35:2260–2264.

26. Lumbroso B, Rispoli M, Savastano MC. Longitudinal optical coherence tomography-angiography study of type 2 naive choroidal neovascularization early response after treatment. *Retina*. 2015;35:2242–2251.

Investigative Ophthalmology & Visual Science